

# CSES IGRF 2020 candidate model for IGRF-13

This note is to provide the information requested to accompany the CSES-based IGRF 2020 candidate model that our ICD-led team wishes to submit for consideration for IGRF-13.

## 1) Team

### *Lead Institution:*

Institute of Crustal Dynamics, China Earthquake Administration (ICD)

### *Secondary Lead Institution:*

Institut de Physique du Globe de Paris/Université de Paris (IPGP)

### *Participating Institutions:*

National Space Science Center, Chinese Academy of Sciences (NSSC)

Space Research Institute, Austrian Academy of Sciences (IWF)

Danish Technical University (DTU)

Hebei GEO University (GEO)

Institute of Earthquake Forecasting, China Earthquake Administration (IEF)

Institute of Geophysics, China Earthquake Administration (IG)

*Team leader:* Yanyan Yang (ICD)

*Secondary team leaders:* P. Vigneron (IPGP), G. Hulot (IPGP)

*Team members:* Xuhui Shen (ICD), Zhima Zeren (ICD), Bin Zhou (NSSC), Magnes Werner (IWF), Nils Olsen (DTU), Lars Toffner-Clausen (DTU), Jianpin Huang (ICD), Feng Guo (ICD), Jingbo Yu (GEO, ICD), Jie Wang (ICD), Yingyan Wu (IEF), Xudong Zhao (IG)

## 2) Data used

**Data type and version:** Data are of two types.

*Type 1:* Level 2 scientific data of the sun-synchronous (descending local time 14:00) China Seismo-Electromagnetic LEO (507 km altitude, circular) Satellite (CSES, Shen et al. 2018) high precision magnetometer package (HPM, Cheng et al. 2018). As can be seen in Figure 1, this HPM package consists of two fluxgate magnetometers (FGM\_S1 and FGM\_S2) and a coupled dark state magnetometer (CDSM, Pollinger et al. 2018). All instruments are located on a deployable boom with two hinges. The CDSM provides the scalar data for both science applications and calibrations of the FGMs. These instruments are jointly providing magnetic field vector and scalar measurement from DC to 15Hz. For the purpose of building the proposed candidate model, the data used are data version 1.0 calibrated using the procedure described in Zhou et al. (2018), and provided by the Institute of Crustal Dynamic, China Earthquake Administration. We only use 1 Hz data, and vector data from the FGM\_S1 instrument, as this instrument proved to be better suited, for reasons explained below. In addition, quaternions providing attitude of the satellite using star cameras located on the body of the satellite are also used. Such nominal data are only available for geographic latitudes between 65°S and 65°N.

*Type 2:* Additional CDSM scalar data were also made available for North and South geographic latitudes higher than 65°. It should be stressed that the main goal of the CSES mission not being main field modelling, such data were not originally planned to be acquired and made available. In addition, the way the CSES mission is being operated implies that most magnetically noisy operations/manoeuvres take place during these high latitude orbital segments. Following the post-launch decision to test the possibility of building an IGRF candidate model entirely based on CSES data, however, a special effort has been made to make such data available. This high-latitude dataset underwent non-nominal dedicated processing, starting from available satellite level data and using GPS time to timestamp the data, in particular. To avoid the most spurious data, these processed data were next screened to ensure that no intensity data departed from the CHAOS6-x9 model by more than 300 nT.

All data of both types collected in this way were next made available to the modelling team, which next screened and selected the data in the way described below.

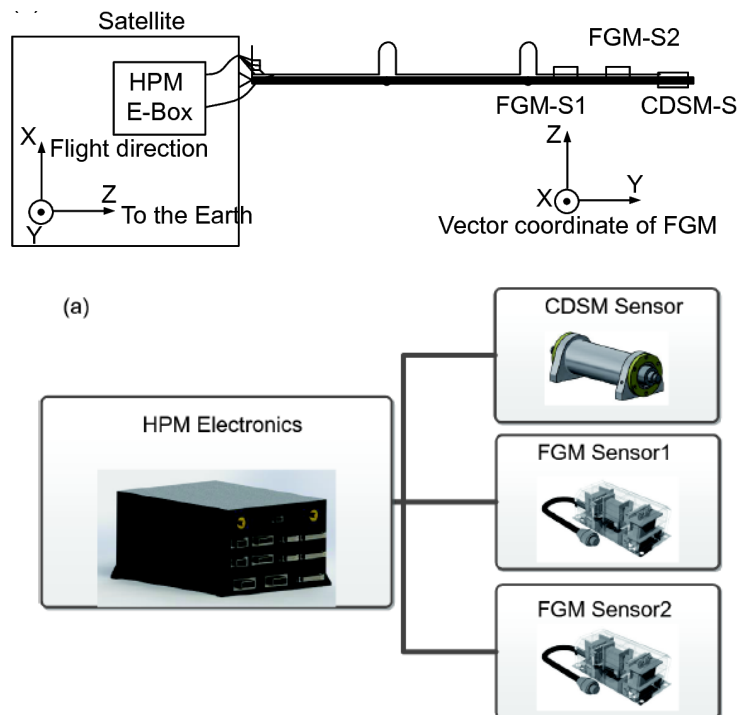


**Figure 1:** Location of the various magnetometers on the CSES satellite. The scalar CDSM and the two fluxgate magnetometers (FGM-S1 and FGM-S2) are located on a deployable boom with two hinges (from Cheng et al., 2018).

**Data temporal distribution:** First data used is from 03/03/2018, last data used is from 20/09/2019 (almost 19 months).

**Data selection:** Data selection criteria are similar to those typically used for dedicated internal field modelling (see e.g. Hulot et al., 2015, where some of the quantities used below are defined) with some special specificities related to the CSES mission. In particular, preliminary investigations made it very clear that the mechanical stability of the boom and hinges (mechanically linking the FGM instruments to the STRs on the body of the satellite) was fairly limited, with significant boom deformation occurring every time the satellite emerges from the dayside, mostly affecting the initial part of the ascending night side (02h00 LT) orbits legs that we used. This led us to restrict use of vector data only within (absolute) QD latitudes of less than  $20^\circ$ , and to assume a fairly large uncertainty (100 arc seconds) on attitude provided by the quaternions.

Data selection criteria can be summarized in the following way:

*Selection common to all data:*

- Sun angle at least  $10^\circ$  below horizon
- Magnetically quiet conditions (based on  $RC < 2\text{nT/h}$  and  $Kp < 2+$ ) are required
- All data were screened to remove any data not satisfying the criteria that differences between each datum and the prediction from CHAOS-6x9 should be less than 100 nT (scalar or norm comparison)

*Additional selection for scalar data:*

- A dedicated Flag signaling when magnetotorquers are on was provided with the data and used to avoid data at times of magnetotorquer activation for all type 1 data (Flag MT should be 0). This flag was not used for type 2 data, as too many data appeared to be affected.
- $E_m < 0.8\text{ mV/m}$  for high latitude scalar data
- Decimation : 1 point every 100 points for type 1 data, no decimation for type 2 data

#### Additional selection for vector data:

- Only vector data for (absolute) QD latitudes less than  $20^\circ$  are selected
- Scalar residuals (difference between scalar and modulus of vector) must be less than 2.5 nT
- 17 days of very problematic data were discarded: 04/05/18, 08/05/18, 12/05/18, 14/05/18, 18/05/18, 20/05/18, 27/05/18, 29/05/18, 30/05/18, 31/05/18, 05/06/18, 12/06/18, 13/06/18, 14/06/18, 24/09/18, 03/03/19 and 20/09/19
- A final decimation (1 out of 15 data points) is being used to avoid over-representation along tracks.

This resulted in the selection of **92 068 scalar data** (among which 62 715 data at absolute geographic latitudes higher than  $65^\circ$ ) and **122 867 x 3 vector data**, distributed in time and latitude as illustrated in Figure 2.

### 3) Parent model parameterization:

The model parameterization used is very similar to the one used in Hulot et al. (2015). It involves a grand total of **640** coefficients corresponding to:

- Time-varying internal field up to degree and order 8 (included), using a simple linear secular variation. This led to  $2 \times 8 \times (8+2) = 160$  coefficients
  - Static internal field between degree and order 9 (included) and degree and order 15 (included). This led to an additional  $15(15+2) - 8(8+2) = 175$  coefficients
  - External field modelled as in Hulot et al. (2015, where details can be found):
    - Remote magnetospheric sources :  $q_n^{0,GSM}$  in GSM frame, with  $n=1,2 \rightarrow 2$  coefficients
    - Near magnetospheric ring current :
      - up to degree and order 2 in SM frame  $\rightarrow 8$  coefficients
      - $\Delta q$  estimated every 5 days for  $q_{10}$  (98 time segments,  $\rightarrow 98$  coefficients)
      - $\Delta q$  estimated every 30 days for  $q_{s11}$  (19 time segments,  $\rightarrow 2 \times 19 = 38$  coefficients)
- Leading to a total of  $2+8+98+38 = 146$  coefficients
- Euler angles (rotation between FGM\_S1 and STR reference frames) estimated every 10 days : 53 time segments,  $\rightarrow 3 \times 53 = 159$  coefficients

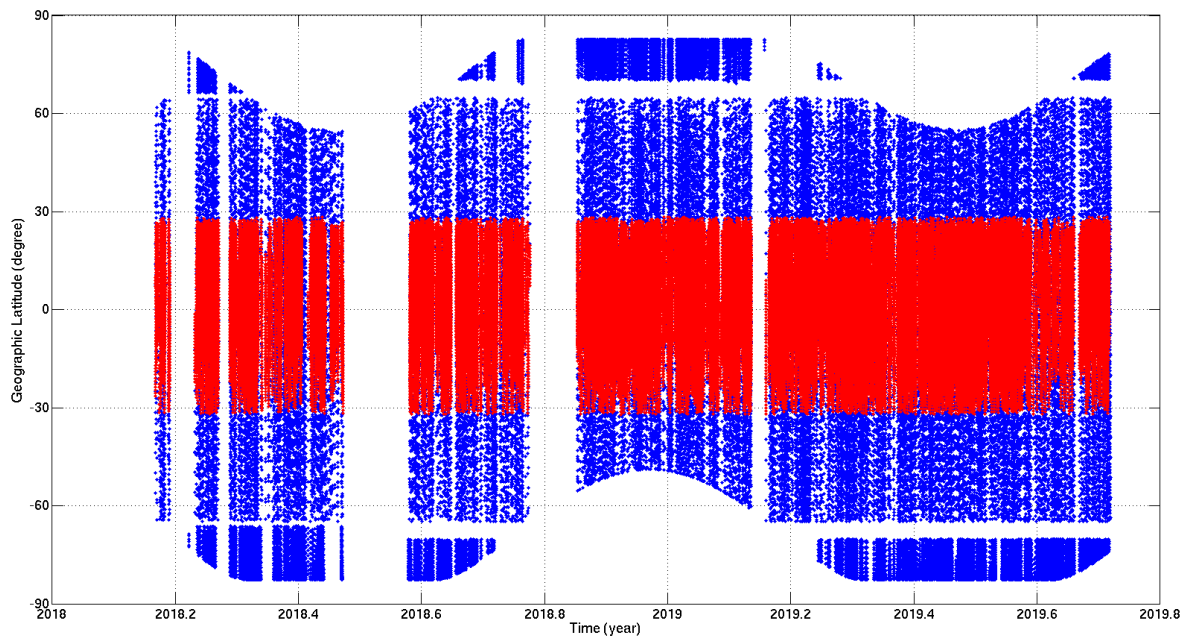


**Figure 2:** Data distribution as a function of time and latitude (blue: scalar data; red: vector data)

### 4) Parent model optimization:

The model was computed as in Hulot et al. (2015) by minimizing the mismatch between data and model prediction, using iteratively reweighted least-squares with Huber weights, without any regularization. Also as in Hulot et al. (2015), a geographical weight was introduced, proportional to  $\sin(\theta)$  (where  $\theta$  is the geographic colatitude), to balance the geographical sampling of data. Anisotropic magnetic errors due to

attitude uncertainty were taken into account assuming an isotropic attitude error of 100 arcsecs to account for the limited quality attitude restitution (recall, indeed, that even isotropic attitude error produces anisotropic magnetic errors, see Holme and Bloxham (1996), the formalism of which we rely on). A priori data error variances were otherwise set to 2.2 nT for both scalar and vector data. The starting model used is a static model (CHAOS-4 up to degree and order 13 only for epoch 01/03/18), but this choice was found to not have any influence on the final model.

A total of eight iterations were used, which was found to ensure convergence to within the accuracy required.

Resulting residual statistics are shown in Table 1.

	number	Raw residuals (mean / std in nT)		Huber Weight residuals (mean / std in nT)		Sum of ponderation
F (polar) [nT]:	30246	0.26	11.76	-0.02	6.20	0.64
F+B_B [nT]:	214935	0.39	5.24	0.26	3.16	0.89
F+B_B low lat :	184689	0.42	3.05	0.29	2.60	0.93
B_B [nT]:	122867	0.64	3.14	0.47	2.67	0.92
B_r [nT]:	122867	0.00	8.32	0.06	8.08	1.00
B_theta [nT]:	122867	-0.70	4.84	-0.70	4.84	1.00
B_phi [nT]:	122867	-0.07	6.05	0.05	5.47	0.97

**Table 1:** Residual statistics for all data used to produce the parent model (using the same convention as in Hulot et al., 2015). *B\_B* refers to vector residuals projected along the field direction; “Low lat” refers to data within (absolute) QD latitude 55°; *F (polar)* refers to scalar data above (absolute) QD latitude 55°.

## 5) IGRF 2020 candidate model generation

The IGRF 2020 candidate model is just the parent model extrapolated to epoch 2020.0 (using its own SV component) and truncated up to degree 13.

## 6) Initial validation

To validate our candidate model, we decided to rely on some comparison of the prediction of our parent model with that of the CHAOS6-x9 model of Finlay et al. (2016). This CHAOS6-x9 model was computed by DTU only using L1b Swarm data (plus data from earlier missions as well as data from ground observatories) and is therefore completely independent. But since it only uses data up to April 2019, comparisons of predictions for epoch 2020.0 was not considered appropriate. In contrast, it can be considered to provide a very reliable estimate of the main field for two epochs of high interest, epoch 11/12/2018, which corresponds to the central time of our parent model, and 20/11/2017, which is 103 days before the very first data used in our parent model. This is the same amount of time separating the last data used in our parent model and epoch 2020.0. Given the symmetry of the CSES data distribution we used (recall Figure 2), we consider this backward extrapolation test as a good test of how well our IGRF 2020.0 candidate model will likely perform.

Figure 3 illustrates the difference in the  $B_r$  values predicted by our CSES parent model and CHAOS6-x9 at Earth’s surface, for central epoch 11/12/2018. As can be seen most differences are of zonal nature, with amplitudes of about 20nT. These differences most likely reflect some of the systematic boom deformation along the CSES orbits. We note, however, that such differences remain within a reasonable acceptable level for typical IGRF candidate models. This, however, needed to be confirmed also in the more realistic case of the backward extrapolation to epoch 20/11/2017. This is illustrated in Figure 4. As expected, errors are now larger, with amplitudes nearly reaching 40nT. But we again note that such differences are

quite comparable (though more of the high side) to differences observed between the various IGRF 2015 candidate models that were proposed in 2015 (at a similar stage of IGRF model preparation). This can be seen by comparing Figure 4 with Figure 7 of Thébault et al., (2015). Note however that in the latter Figure, colour scales are saturated, which partly limits the comparison.

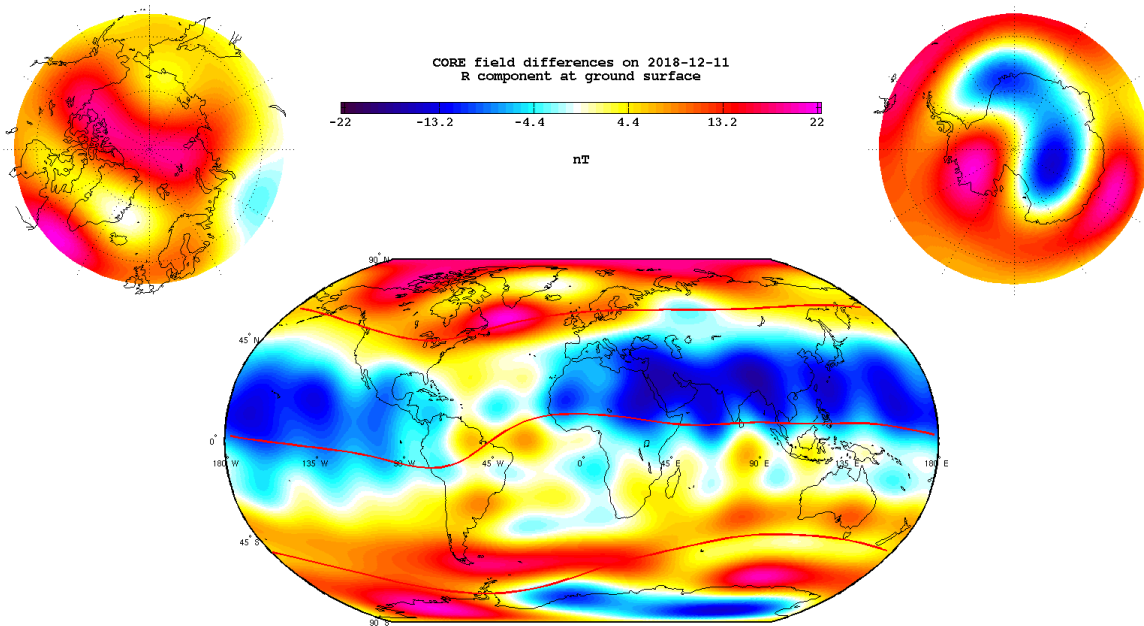


Figure 3: Difference in the  $B_r$  values predicted by our CSES parent model and CHAOS6-x9 at Earth's surface for central epoch 11/12/2018.

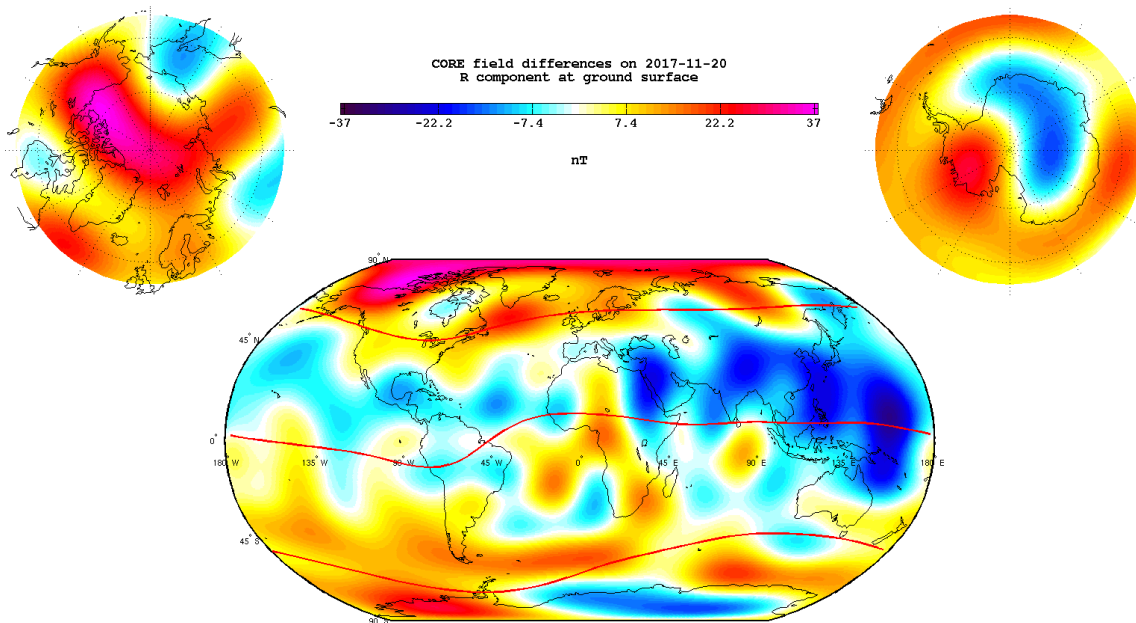


Figure 4: Difference in the  $B_r$  values predicted by our CSES parent model and CHAOS6-x9 at Earth's surface for backward extrapolated epoch 20/11/2017.

To further illustrate the likely quality of our CSES IGRF 2020.0 candidate model, we also computed the Lowes-Mauersberger spectra of the differences between our CSES parent model and CHAOS6-x9 for central epoch 11/12/2018 (Figure 5) and backward extrapolated epoch 20/11/2017 (Figure 6). These spectra lead to the same orders of magnitude for the disagreements between the two models as illustrated in Figures 3 and 4. They also highlight the fact that disagreements are strongest for degrees 1 to 3, corresponding to the large-scale zonal structures seen in Figures 3 and 4. Focussing on the backward extrapolated epoch 20/11/2017, best representative of the likely error affecting our CSES IGRF 2020.0 candidate model (which, we recall amount to forwarding our CSES parent model over an identical period

of time), we can see that this spectral error can be expected to reach  $20 \text{ nT}^2$  for degree 1,  $50 \text{ nT}^2$  for degree 2,  $30 \text{ nT}^2$  for degree 3 while remaining well below  $10 \text{ nT}^2$  for all higher degrees, except for degree 9, again reaching  $20 \text{ nT}^2$ . We again interpret the strongest disagreements for degrees 1 to 3 as a likely consequence of some systematic boom deformation along the CSES orbits.

These disagreements clearly show that the current quality of CSES data for IGRF modelling purposes is most likely limited by the boom deformation issue, which we could only partly mitigate by restricting the use of vector data at absolute QD latitudes below  $20^\circ$ , and most likely also, by the still limited quality of the scalar polar latitude data (type 2, as can also be seen by shear inspection of the corresponding residual statistics in Table 1).

Nevertheless, we also note that the observed disagreements for the backward extrapolated epoch 20/11/2017, indicative of the likely quality of our CSES IGRF 2020.0 candidate, is within reasonable range (though on the high edge for degrees 1 to 3) of the type of disagreements previously observed among IGRF 2015.0 candidate models (see Figure 4 of Thébault et al., 2016).

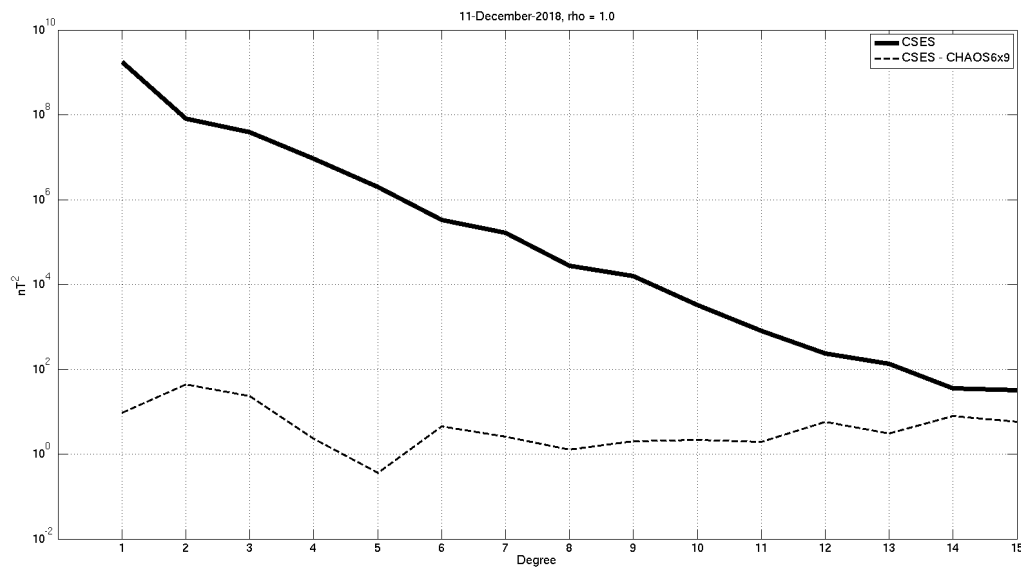


**Figure 5:** Spectra of our CSES parent model (black solid line, referred to as CSES) and of the difference between our CSES parent model and the CHAOS6-x9 model (black dashed line, referred to as CSES - CHAOS6x9) for central epoch 11/12/2018, both at Earth's surface.

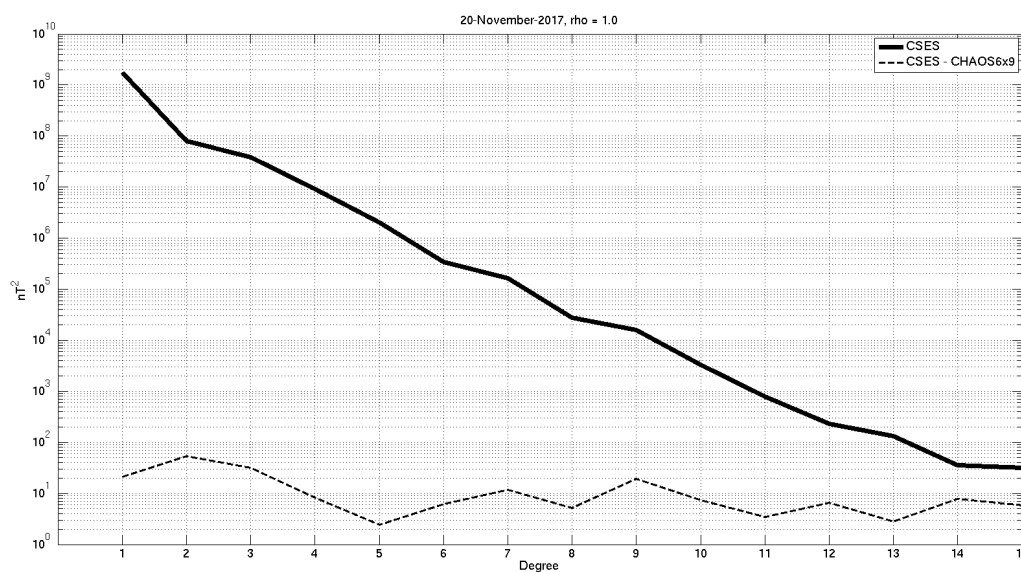


**Figure 6:** Same as Figure 5, but for backward extrapolated epoch 20/11/2017.

## 7) Computation of realistic uncertainties on each Gauss coefficient

To compute “realistic” uncertainties affecting the Gauss coefficients of our CSES IGRF 2020 candidate model, the following simple strategy was used. We again assumed that the observed disagreements between the CSES model backward extrapolated to epoch 20/11/2017 (using the CSES parent model) and the CHAOS6-x9 model computed at the same epoch, could be representative of the type of errors one can expect in the CSES IGRF 2020 candidate model.

For each degree  $n$ , we then simply computed the following RMS quantity:

$$\sigma_n = \text{sqrt} [ (\sum \{ dg_n^2 + dh_n^2 \}) / (2n+1) ],$$

where  $dg_n$  and  $dh_n$  are the differences in the  $g_n$  and  $h_n$  Gauss coefficients from the two models.

We then simply assigned this  $\sigma_n$  as our best estimate of the errors (one sigma type) affecting each Gauss coefficient of degree  $n$ .

We admit that this method is probably a bit rough, and note that it likely underestimates uncertainties affecting zonal coefficients (i.e.  $g_n^0$  Gauss coefficients), by probably a factor 2 (at least for degrees 1 to 3, recall discussion in section 6 above).

## 8) Conclusion

Given the first assessment provided in this note, we conclude that our CSES IGRF 2020 candidate model entirely based on CSES data, though not devoid of limitations, is a decent independent candidate that could be used for contribution to the final IGRF 2020 model.

## 9) References:

- Cheng B. J., Zhou B., Magnes W., et al., High precision magnetometer for geomagnetic exploration onboard of the China Seismo-Electromagnetic Satellite, *Sci China Tech Sci*, 61: 659–668, <https://doi.org/10.1007/s11431-018-9247-6>, 2018.
- Finlay, C.C., Olsen, N., Kotsiaros, S., Gillet, N., Tøffner-Clausen, L., Recent geomagnetic secular variation from *Swarm* and ground observatories as estimated in the CHAOS-6 geomagnetic field model, *Earth Planets Space*, 68 : 112, <https://doi.org/10.1186/s40623-016-0486-1>, 2016. For the CHAOS-6-x9 version of this model, see <http://www.spacecenter.dk/files/magnetic-models/CHAOS-6/>.
- Hulot, G., Vigneron, P., Léger, J.-M., Fratter, I., Olsen, N., Jager, T., Bertrand, F., Brocco, L., Sirol, O., Lalanne, X., Boness, A., Cattin, V., *Swarm's absolute magnetometer experimental vector mode, an innovative capability for space magnetometry*, *Geophys. Res. Lett.*, 42, <https://doi.org/10.1002/2014GL062700>, 2015.
- Holme, R., and J. Bloxham, The treatment of attitude errors in satellite geomagnetic data, *Phys. Earth Planet. Inter.*, 98, 221–233, 1996.
- Pollinger A., Lammegger R, Magnes W, et al., Coupled dark state magnetometer for the China seismo-electromagnetic satellite, *Meas. Sci. Technol*, 29, 095103, <https://doi.org/10.1088/1361-6501/aacde4>, 2018.
- Shen X. H., Zhang X. M., Yuan S. G., et al., The state-of-the-art of the China Seismo-Electromagnetic Satellite mission, *Sci China Tech Sci*, 61: 634–642, <https://doi.org/10.1007/s11431-018-9242-0>, 2018
- Zhou, B., Yang, Y. Y., Zhang, Y. T., Gou, X. C., Cheng, B. J., Wang, J. D., and Li, L., Magnetic field data processing methods of the China Seismo-Electromagnetic Satellite. *Earth Planet. Phys.*, 2(6), 455–461, <http://doi.org/10.26464/epp2018043>, 2018.